Case Studies in Construction Materials 18 (2023) e01813

Contents lists available at ScienceDirect

Case Studies in Construction Materials

journal homepage: www.elsevier.com/locate/cscm

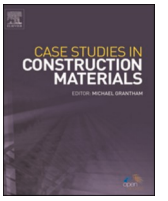

Case study

Durability enhancement of half-joints in RC bridges through external prestressed tendons: The Musmeci Bridge's case study

Giuseppe Santarsiero *, Valentina Picciano

School of Engineering, University of Basilicata, Viale dell'ateneo lucano 10, 85100 Potenza, Italy

ARTICLE INFO

Keywords:
RC bridge
Half-joints
Finite element
External post-tension
Durability analysis
Chloride corrosion

ABSTRACT

This paper numerically investigates the effect of post-tension interventions to strengthen the deteriorated half-joints of the Musmeci Bridge in Potenza (Italy), with the primary objective of increasing the ultimate load-bearing capacity and monitoring the secondary effects in terms of preventing or limiting cracking patterns. Bearing this in mind, the study aims to investigate the role of the reinforcement detailing, of the post-tension stress and of the corroding time in the presence of chlorides, outlining the intervention ability to improve the structure's durability. To this end, nonlinear finite element models are provided with chloride ions diffusion analysis to investigate corrosion initiation and progress in reinforced concrete elements and account for deterioration due to two scenarios (45 and 95 years). Results show the significant impact of reinforcement layout as the presence of inclined bars increases the ultimate load by about 86 %. The ultimate load improvement is in the range 50–55 % when the intervention is carried out after 45 years while it is equal to about 30–35 % if a period of 95 years is last since the construction. This latter highlights the significant influence of the intervention timeliness on structural durability.

1. Introduction

Old bridges have suffered a significant increase in traffic loads as well as in their frequency which determines heavier loading conditions compared to design assumptions. Moreover, environmental stresses (e.g., carbonation chloride ingress, freeze-thaw cycles, etc.) caused material deterioration which was accelerated by the lack of ordinary maintenance interventions. The joint effect of material degradation and increased loading conditions is represented by a reduction of durability (i.e., the ability to accomplish their intended purposes for a sufficiently long period, or at least during the expected service life). Huge efforts are needed from the financial point of view to intervene on many bridges constructed after the Second World War using innovative prestressing techniques even though with shallow material properties' control [1]. Therefore, to optimise the use of financial resources for maintaining bridges, effective technical solutions need to be experimentally tested and numerically verified.

Specifically, cantilever bridges were widely used in the past due to their intrinsic advantages linked to the stress distribution coupled with their statically determinate condition. Key components of these bridges are half-joints, where cantilever and suspended spans are connected [2]. These latter are frequently subjected to maintenance issues caused by the water seepage permitted by the deck drainage malfunction leading the platform water to flow through the expansion joints [3], which are frequently in service after losing their waterproof feature. Moreover, in harsh climates, platform water contains de-icing salts responsible for chloride ingress and

* Corresponding author.
E-mail address: giuseppe.santarsiero@unibas.it (G. Santarsiero).

https://doi.org/10.1016/j.cscm.2022.e01813
Received 21 November 2022; Received in revised form 27 December 2022; Accepted 27 December 2022
Available online 29 December 2022

Nomenclature

C_s	Surface chloride concentration.
D_{ref}	Diffusion coefficient.
C_{crit}	Critical chloride content.
t_{ref}	D_{ref} evaluation time.
t_{corr}	Corrosion period.
f_{cm}	Mean compressive strength of concrete.
f_{cd}	Concrete compressive strength.
f_{ctd}	Concrete tensile strength.
E	Young's modulus.
G_F	Fracture energy.
ν	Poisson's coefficient.
f_{yk}	Reinforcement characteristic yielding stress.
f_{yd}	Reinforcement yielding stress.
f_{td}	Reinforcement failure stress.
ε_t	Reinforcement failure strain.
CF	Confidence factor.
γ_m	Material partial factor.
f_y	Yielding stress of tendons' steel.
f_t	Failure stress of tendons' steel.
f_{ys}	Yielding stress of ordinary steel.
f_{ts}	Failure stress of ordinary steel.
a	Restraining plates width.
b	Restraining plates length.
h	Restraining plates thickness.
d	Half-joint vertical deflection.
P_s	Service load.
F_p	Total tendons'load.
σ_p	Tendons' stress.
σ_c	Post-tension compressive stress on concrete.
w_{max}	Max crack width under service load.
Δw_{max}	Variation of w_{max}.
P_c	Cracking load.
ΔP_c	Variation of cracking load.
P_u	Ultimate load.
ΔP_u	Variation of ultimate load.
d_u	Ultimate deflection.
Δd_u	Variation of ultimate deflection.
K_{sec}	Secant stiffness.

related corrosion mechanisms [4,5]. It is worth noting that polluted water flowing through the joints also affects the efficiency of bearings, causing huge deterioration that can, in turn, increase issues on half-joints.

Therefore, in most cantilever bridges, half-joints represent the main problem in view of the whole structure's safety as their degradation can lead to significant performance reduction and, in some cases, cause failure [6].

In this framework, some authors used simplified methods to evaluate the residual load-bearing capacity of half-joints accounting for deterioration mechanisms [8,9]. More refined methods for the prediction of corrosion progression along with the associated structural behaviour would be a helpful tool in the maintenance scheduling and retrofit intervention design of such components. This task can benefit from mechano-chemical approaches, which allow for performing durability analyses, leading to the assessment of bridges and their components as a function of time accounting for corrosion degradation. Specifically, the evaluation of chloride ions' effect is based on a set of parameters describing the aggressivity of the surrounding environment and the concrete sensitivity to the chloride content in becoming a corrosion-prone medium for the embedded steel reinforcement. These parameters can be chosen as deterministic [7] or based on stochastic approaches allowing refined reliability analyses [10,11].

Besides the performance evaluation of bridge half-joints accounting for corrosion, a major relevance is played by the availability of suitable retrofitting techniques, possibly low-impact and cheap. Several studies investigated techniques to improve the half-joint performance related to several structures such as slabs, roofs, and bridges.

For instance, several studies were devoted to investigating the feasibility and the effectiveness of strengthening interventions made by composite materials aimed to improve the shear and flexure strength of reinforced or plain concrete elements with various carbon fibre sheets' configurations [12,13]. In the study of Ref. [14], half-joints belonging to prestressed concrete double tee beams were

experimentally investigated. The tests showed the performances of half-joints reinforced with externally bonded carbon fibre laminates and those of similar elements with improved reinforcement detailing. It is worth noting that the investigated elements (double tee beams) are commonly used in either roofs or slabs, and results cannot be directly extended to bridges. Taher [15] reported the results of different CFRP wrapping configurations applied to dapped-end beams. The strengthening configurations differ in terms of inclination with respect to the beam axis and the extent of application (only the nib, the full depth part, or both regions). The study found strength increments of around 40 %.

In [16] the authors conducted static tests on RC half-joints belonging to roof beams retrofitted with FRP-based strengthening techniques to delay the collapse according to failure mode 3 [17] (diagonal crack starting from the re-entrant corner). The results showed that FRP laminates applied along the half-joint corner remarkably improved the cracking load (around 116 %). However, due to debonding issues, the ultimate load was improved by only 10 %.

Atta and Taman [18] tested eight reinforced concrete beam specimens provided with dapped ends and upgraded through several post-tension techniques made by steel rods having different inclinations. Three solutions provided more remarkable performance improvements concerning the load-bearing capacity. For instance, a couple of prestressed tendons applied near the re-entrant corner of the half-joint can improve the ultimate load by about 65 %. However, this study considered only one prestress value and the effects of its possible variation were not investigated.

Both composite-based and post-tension-based techniques were tested only on specimens without inclined bars, whose presence is rather widespread in the reinforcement layout of European bridges' half-joints [7,19,20].

Based on the above-cited studies, post-tension techniques are able to provide significant improvement in terms of both cracking and ultimate load-bearing capacity, and for this reason, they deserve additional investigation. Specifically, further research should be devoted to half-joints provided with inclined rebars. To this end, the present study is devoted to numerically investigating a post-tension retrofitting solution applied to a case study bridge's half-joint [21,22]. The goal is to examine the effect of corrosion time, post-tension stress, and the presence/absence of inclined bars in the reinforcement layout in order to cover the mentioned research gaps and provide owners and practitioners with practical suggestions for the design of rehabilitation interventions.

In fact, post-tension techniques using steel elements are suitable as retrofitting systems for half-joints belonging to bridges, since they match the geometrical requirements in Gerber bridge structures.

The feasibility of retrofitting interventions through different systems and materials plays a key role in refurbishment interventions [2], for instance, the major limitation to the application of externally bonded composites is represented by the presence of the curb and the transverse beam connecting the main girders. Therefore, post-tension techniques are usually the most suitable for a bridge's half-joints since they do not need the girders' sides to be clear. This kind of intervention has been carried out on real bridges [19,23] and on experimentally tested specimens [18], being rather simple to implement.

Holes are drilled near the girder sides in correspondence of the edge of the undapped region (Figs. 1a and 1b). The eventual curb and transverse beam must be perforated too.

Then, high-strength steel rods are placed and fastened on top and bottom steel plates. Finally, the design prestress force F_p (being the sum of the two ties' forces) must be applied to the rods in order to make them active in improving the structural performance of the half-joint at hand. According to [17], five possible failure modes can be observed in half-joints, depicted in Fig. 2.

As can be seen, applying the force F_p on the opposed bottom and top sides of the undapped girder region directly prevents the opening of inclined cracks according to failure modes 3 and 5. A broad literature analysis [8,9,14,18,24–34] regarding 141 experimental tests on half-joints revealed that failures involving modes 3 and 5 are the most frequent. Globally, failures involving modes 3 and/or 5 occur in 75.2 % of the analysed specimens, indicating that post-tension interventions could be effective in a wide range of RC half-joints [35].

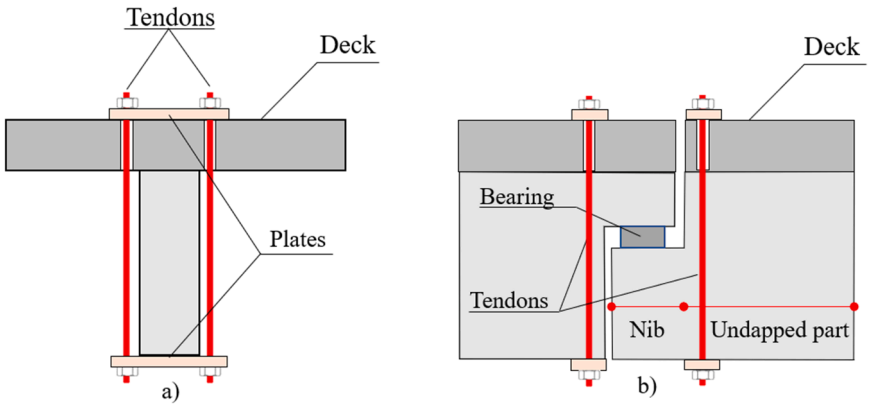

Fig. 1. External tendons layout on a bridge half-joint.

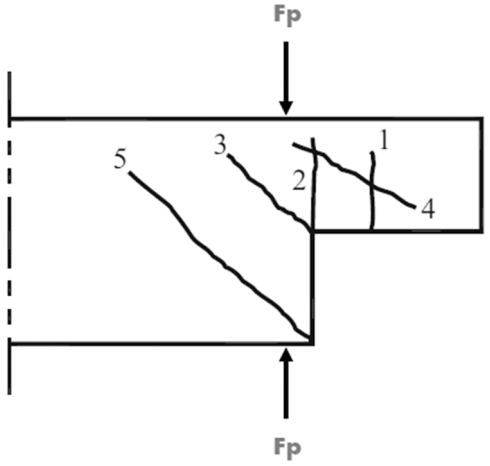

Fig. 2. Failure modes of half-joints according to [17]: 1 = Nib flexure crack; 2 = Direct shear crack; 3 = Re-entrant corner crack; 4 = Nib inclined crack; 5 = Diagonal tension crack.

2. The case study bridge

The case study bridge already described in [7,21,22], was designed by Sergio Musmeci (today called Musmeci Bridge) matching older codes [36]. Its RC box deck is 16 m wide and supported by the vault every 17.30 m for a total length of 300 m (Fig. 3). The deck is supported by a double-curvature RC vault designed through a form finding study devoted to optimising the stress flow and exploit the concrete ability to support compression stress fields (Fig. 3a).

The deck is provided with suspended spans (10.38 m long) connected by half-joints which are located in the position shown in detail in Fig. 3b. Structural details of half-joints as reported in the original design drawings are shown in Fig. 4. As can be seen, the half-joints are provided with inclined bars in addition to the horizontal and vertical ones near the corners of the dapped parts, where the bearing is placed. Previous research [9] demonstrated the great impact of reinforcement layouts, highlighting the increase in the load-bearing capacity of these kinds of elements depending on the presence of inclined bars. Therefore, the following numerical investigation is related to both the case of the presence and absence of such reinforcement in order to obtain more general results somehow applicable to a wider stock of bridges.

3. Numerical investigation

Nonlinear FEM models were developed to accurately simulate the mechanical response of half-joints accounting for the complex behaviour of reinforced concrete structures due to the brittle and non-isotropic behaviour of concrete. This was made in the ATENA software environment [46] which incorporates the nonlinear fracture mechanics theory, being able to predict both tension cracking and compression crushing of concrete. The concrete volume is simulated mainly by hexahedral elements (brick type) and prismatic elements in the transition zone (red-coloured region in Fig. 5). All the steel plates for constraining the model and the prestressing bars are meshed with tetrahedral elements. All reinforcement bars are modelled through 1D truss elements embedded in concrete elements.

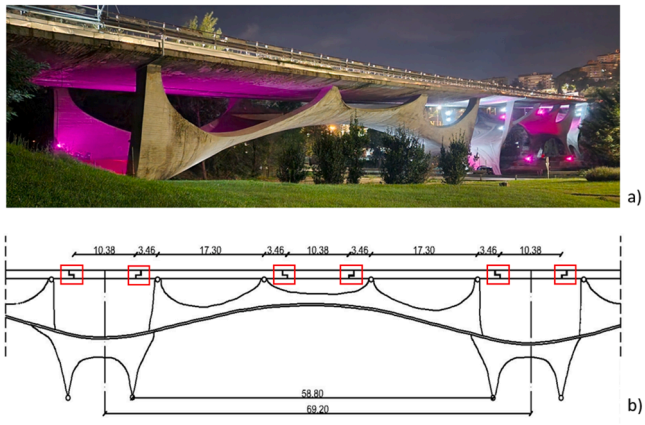

Fig. 3. Musmeci Bridge's overview (a) and structural scheme of a span (b) (dimensions in m).

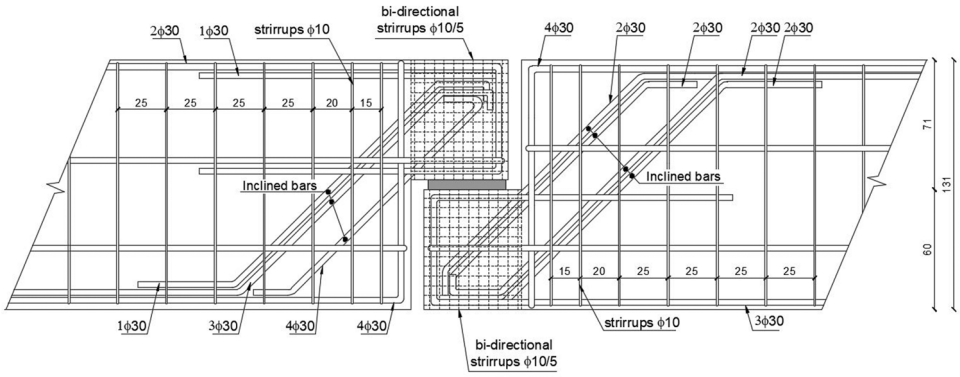

Fig. 4. Musmeci Bridge's half-joints (dimensions in cm).

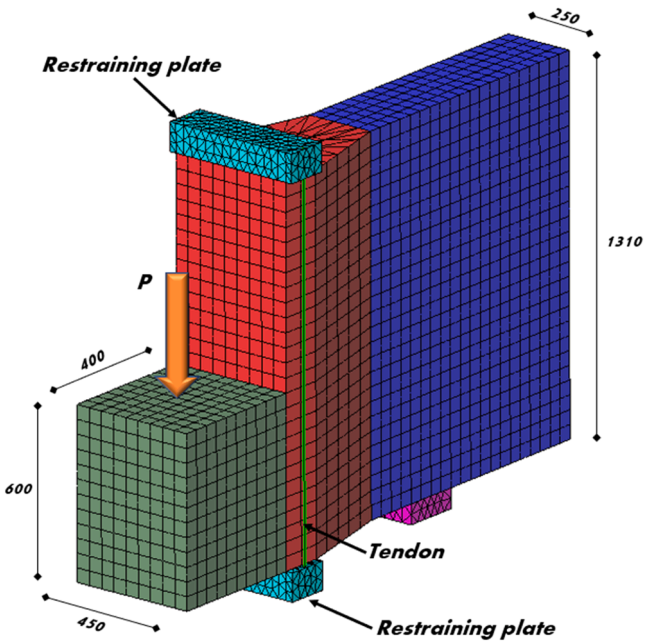

Fig. 5. FEM model provided with the strengthening system (dimensions in mm).

Perfect connection is assumed between concrete and steel as an acceptable choice due to the negligible bond deterioration that occurs in the case of monotonic loading.

Beyond the detailed structural response of the investigated half-joints, the software incorporates the capability of simulating chloride ingress inside the concrete volume, and detect corrosion initiation and progression so as to estimate reinforcement mass loss at any time and the related performance degradation of the whole structure. The corrosion effects are related to the cracking patterns due to service loads. This means that the corrosion modelling considers the presence of cracks and their effects in accelerating the chloride ingress.

In fact, recent studies explicitly included corrosion modelling in the evaluation of existing bridges [37–39]. This is particularly helpful for half-joints which, due to their shape, cannot be inspected properly and an estimate of the corrosion extent is needed. As an example, the study in [7] was conducted through detailed numerical investigations on a bridge's half-joints to detect the effect of chloride-induced corrosion on the load-bearing capacity. To this end, a mechano-chemical approach [40] was used to account simultaneously for the mechanical (service loads) and environmental (chloride penetration due to de-icing salts) actions.

The considered service load is the structure's self-weight while the definition of the corrosion attack is based on the chloride ions ingress modelled according to a 1D diffusivity approach based on the second Fick's law [41]. This latter needs a set of three parameters to model the chloride penetration inside the concrete volume: (i) surface chloride concentration C_s (as % of cement mass), (ii) diffusion coefficient D_{ref} (m^2/s) evaluated after t_{ref} years and (iii) critical chloride content C_{crit} (as % of cement mass). A detailed discussion of the meaning of these corrosion parameters can be found in [40]. In fact, the degradation model assumes that corrosion starts when chloride concentration near the reinforcement exceeds the critical value $C_{crit.}$ Chloride ions move in only one direction (1D model)

normal to the concrete surface where chloride ions are present with a concentration equal to C_s.

The study in [7] also considered several possible combinations of values of these parameters [38,42–44] to find the worst one in terms of corrosion and load-bearing capacity loss. This latter is the one used in this study, based on the highest value of C_s and D_{ref}, and the lowest one of C_{crit}. Therefore, the environmental conditions can be considered very aggressive with respect to road bridges in harsh climates with extensive use of de-icing salts.

Based on the corrosion environment, an external post-tension intervention is modelled to assess the effects of load-bearing capacity gain and possible changes in the failure mode concerning the as-built condition. Moreover, two possible corroding periods are considered: 45 and 95 years. 45 years is related to the current condition of the bridge (the bridge was completed about 45 years ago) and explores the effects of timely intervention, while 95 years is investigated to find out what happens if the strengthening is applied after 50 years of additional corrosion time. An additional parameter for the subsequent analyses is the presence of the inclined 30 mm diameter bars in the reinforcement layout. Given that the Musmeci Bridge's half-joints are equipped with inclined bars, it is also helpful investigating the condition of their absence in order to assess the effectiveness of the proposed intervention for a wider range of real bridges.

The intervention is made by two external steel post-tensioned bars (one on each beam's side) according to the solution applied to specimen no. 3 by Atta and Taman [18]. These bars are installed using holes drilled through the transverse beam connecting the beams. Restraining steel plates are necessary at the bottom and top of the beam (Fig. 5) to fasten the bars' ends.

All the modelling choices related to concrete and reinforcing steel in the framework of the nonlinear fracture mechanics approach adopted in the previously mentioned numerical analyses are detailed in the previous works [7,45].

It is worth remembering that numerical models are generated with ATENA software [46] which can account for concrete crushing in compression [47] and cracking in tension, based on an exponential softening of concrete tensile strength [48], as well as the cracking effect related to the chloride diffusion according to 2nd Fick's law [40].

Nonlinear finite element modelling of existing structures is to be carried out referring to material (reinforcing steel and concrete) design strength values evaluated according to [39] which is the current code for existing bridge safety assessment in Italy. This latter accounts for both mean f_m and characteristic f_k values and confidence factor CF depending on the knowledge level achieved during the in-situ testing campaign, as follows:

$$f_d = \min\left(\frac{f_m}{CF \bullet \gamma_m}; \frac{f_k}{CF}\right) \tag{1}$$

where γ_m is the material partial factor. When experimental tests on reinforcing steel are unavailable (as in this case study), the mean value f_m is unknown, and the characteristic value (Table 2) has been used in Eq. (1). This provides a design value f_{yd} equal to the characteristic one, assuming $CF = 1$ (maximum knowledge level, KL3). As for concrete, the mean value is available (Table 1) from a previous cores' extraction campaign, the design value is $f_{cd} = f_m/(CF \cdot \gamma_m)$.

Regarding the new elements of the rehabilitation system, tendons are made of commercial Dywidag high-strength steel (Table 3), even though they may also be of 10.9 class steel according to [49,50]. The only difference is that the former may be provided with a built-in protection system against corrosion, which would be a desirable feature for such an intervention.

Restraining plates are made of ordinary S275 steel (Table 4). Their thickness h is set to 100 mm in order to limit modelling issues related to possible plates' deflection. In real cases, the plates lie on the bridge's concrete slab and the thickness can be much lower due to the absence of the cantilever part.

The numerical analyses are parameterised concerning the corrosion time t_{corr} and the prestress value σ_p applied to the tendons. Table 5 shows the 11 cases reflected by the numerical analyses. They become 22, considering the analyses carried out on the same model without inclined bars.

As can be seen from Table 5, the tendons stress ranges between zero (absence of intervention) and $0.40f_y$, while t_{corr} possible values are 0 (absence of corrosion), 45 and 95 years.

An important parameter is σ_c, which represents the normal stress between the restraining plates and the underlying concrete, obtained as the ratio between F_p and the plates' surface in contact with the concrete (450×150 mm^2). It is somehow representative of the compression axial load applied by tendons to the concrete region near the re-entrant corner. In their experimental tests, Atta and Taman [18] applied a tendon prestress equal to $0.30f_y$. Considering a different half-joint regarding both its geometry and tendon's features, it is more useful to compare the σ_c values. In fact, in their tests σ_c was equal to 2.77 MPa, which is similar to the case of this study with $\sigma_c = 2.33$ MPa corresponding to a prestress value equal to $\sigma_p/f_y = 0.15$ (see Table 5).

Each mechano-chemical analysis includes four different consecutive intervals:

Table 1
Concrete properties for nonlinear modelling [7].

Mean compressive strength	$f_{cm} = -25.85$ MPa
Design compressive strength	$f_{cd} = -17.24$ MPa
Design tensile strength	$f_{ctd} = 1.59$ MPa
Young's modulus	$E = 29{,}253.88$ MPa
Fracture energy [44]	$G_F = 1.31\text{E-}4$ MN/m
Poisson's coefficient	$\nu = 0.20$

Table 2
Reinforcement properties for nonlinear modelling [7].

Young's modulus	$E = 200$ GPa
Characteristic yielding stress	$f_{yk} = 375$ MPa
Design yielding stress	$f_{yd} = 375$ MPa
Failure stress	$f_{td} = 460$ MPa
Failure strain	$\varepsilon_t = 18$ %

Table 3
Tendon properties.

Steel type	f_y [MPa]	f_t [MPa]	Diameter [mm]	Area [mm^2]
Dywidag	950	1050	26.5	552

Table 4
Restraining plate properties.

Steel class	f_{ys} [MPa]	f_{ts} [MPa]	$a \times b \times h$ [mm^3]
S275JR [49,50]	275	430	$500 \times 150 \times 100$

Table 5
Parametric analysis settings.

Analysis	t_{corr} [years]	σ_p/f_y [–]	Post-tension stress σ_p [MPa]	Post-tension load F_p [kN]	σ_c [MPa]	σ_c/f_{cd} [–]
1	0	0	0	0	0	0
2	45	0	0	0	0	0
3		0.05	47.5	52.4	0.78	0.05
4		0.15	142.5	157.3	2.33	0.14
5		0.30	285.0	314.6	4.66	0.27
6		0.40	380.0	419.5	6.22	0.36
7	95	0	0	0	0	0
8		0.05	47.5	52.4	0.78	0.05
9		0.15	142.5	157.3	2.33	0.14
10		0.30	285.0	314.6	4.66	0.27
11		0.40	380.0	419.5	6.22	0.36
$f_{cd} = 17.24$ MPa						

- Interval 1: application of the vertical load on the nib midpoint. The load is equal to $P_s = 270$ kN and corresponds to the structure's self-weight.
- Interval 2: corrosion analysis. Application on the external half-joint surfaces of the chloride load. This analysis computes the chloride transport towards the steel reinforcement, revealing the corrosion initiation and propagation over time. Static equilibrium is computed after each year of corrosion. At the end of this interval, the deflection and cracking usually increase as steel rebars lose a share of their area.

Table 6
Performance at the serviceability and ultimate limit states as a function of the applied post-tension for the model with inclined bars.

			SLS		ULS	
Analysis	t_{corr}	σ_p/f_y	P_c [kN]	w_{max} [mm]	P_u [kN]	d_u [mm]
1	0	0	693.0	0.0479	1746.62	8.64
2	45 years	0	629.8	0.0521	1637.34	7.59
3		0.05	638.6	0.0486	2042.58	7.53
4		0.15	768.8	0.0419	2056.27	7.41
5		0.30	868.9	0.0343	2054.19	7.1
6		0.40	893.4	0.0301	2049.76	6.93
7	95 years	0	517.1	0.0715	1466.21	9.16
8		0.05	604.4	0.0670	1709.62	7.96
9		0.15	652.9	0.0577	1738.85	7.74
10		0.30	719.9	0.0459	1749.18	7.26
11		0.40	784.7	0.0398	1748.50	6.94

- Interval 3: the retrofit intervention (if any) becomes active, and post-tension is applied through a proper number of steps. Cracking and deflection usually decrease due to compressive stresses applied to the concrete volume.
- Interval 4: displacement-controlled analysis up to failure. The vertical deflection is increased to find the half-joint ultimate load P_u and check the ultimate deflection and related ductility.

It is worth noting that corrosion analysis does not consider the variability of governing parameters C_s, D_{ref} and C_{crit}, but deterministically assumes a triad of values based on literature data [38,42–44] related to bridges exposed to de-icing salts. Specifically, they are equal to $C_s = 2.8$ %, $D_{ref} = 3.28\text{E-}12$ m^2/s and $C_{crit} = 0.4$ %.

4. Analysis of results in the presence of inclined bars

Table 6 shows the main results of parametric analyses. As a function of the applied post-tension value σ_p/f_y, both serviceability (SLS) and ultimate limit state (ULS) results are reported. SLS is evaluated concerning w_{max} which is the maximum crack width after the corrosion period and under the applied service load. As can be seen, this parameter significantly decreases as the post-tension increases, being about half the value in the absence of intervention when $\sigma_p/f_y = 0.40$. This happens for both 45- and 95-years corrosion periods. Moreover, it is important to establish the load P_c for which a crack width equal to the limit value required by the code [50,51] is attained. This latter is equal to 0.20 mm as a function of the environmental aggressivity and steel sensitivity to corrosion. P_c increases more significantly for post-tension values equal or higher than $\sigma_p/f_y = 0.15$. Therefore, performance at SLS is increasing as a function of post-tension values. Graphs in Fig. 6 highlight increases in cracking load P_c and decreases of w_{max} as a function of post-tension, showing that relationships are almost linear. Therefore, increasing the post-tension value has significant effects on serviceability behaviour. These effects are slightly sensitive to the corrosion period after which the post-tension is applied, as the improvement of SLS performance seems to be more remarkable in the case of $t_{corr} = 95$ years especially when higher post-tension stress is used.

Regarding the ULS, it can be noted that the ultimate load P_u already shows a significant improvement when minimum post-tension ($\sigma_p/f_y = 0.05$) is applied. It remains almost the same or shows some decreases for higher post-tension values. This phenomenon is due to earlier concrete crushing for high post-tension loads, stressing the undapped half-joint region.

Variations of the ultimate load and ultimate deflection are displayed in Fig. 7. As can be noted, the improvement of P_u is not significantly sensitive to different values of post-tension. Further, it slightly decreases passing from $\sigma_p/f_y = 0.30$–0.40 (Fig. 7a). Therefore, even quasi-passive tendons effectively increase the ultimate load capacity. Moreover, post-tension interventions are more effective on less degraded structures subjected to a lower loss of steel. In fact, in the case of $t_{corr} = 45$ years, ΔP_u is averagely equal to 25 %, while for $t_{corr} = 95$ years is 18 %.

Regarding the half-joint deformation capacity, as can also be seen from load-deflection curves in Figs. 8a and 8b, models with post-tension show sudden load drop after the peak due to the previously mentioned concrete crushing effects. Ultimate deflection d_u is assumed as the value corresponding to a load drop of 20 %, according to Panagiotakos and Fardis [52].

The ultimate deflection values d_u for the analyses with zero prestress (analyses 2 and 7 in Table 6) are equal to 7.59 mm and 9.16 mm for $t_{corr} = 45$ y and 95 y, respectively. The lower ultimate deflection for $t_{corr} = 45$ y is mainly because this model has a higher steel amount due to the shorter exposure to chlorides.

This determined a failure mechanism involving concrete crushing, as can be seen the failure modes' analysis. However, a progressive increase in post-tension stress leads to higher deflection capacity losses for $t_{corr} = 95$ y (Fig. 8b).

The higher ultimate load improvements and lower losses in ultimate deflection demonstrate that early retrofitting interventions provide significantly better performance, which could lead also to a prolonged structure's lifespan. Graphs of Fig. 8a–b confirm this latter, showing that the post-tension intervention (with any level of prestress) can recover the load-bearing capacity lost with corrosion

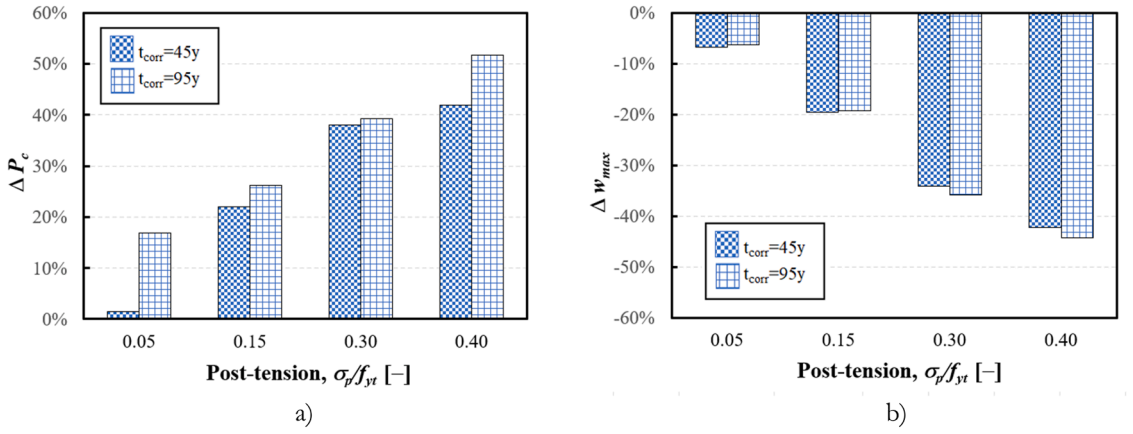

Fig. 6. Variations of cracking load (a) and maximum crack width under service loads (b) for retrofitted models after 45 years and 95 years of corrosion compared to the as-built corroded models (with inclined bars).

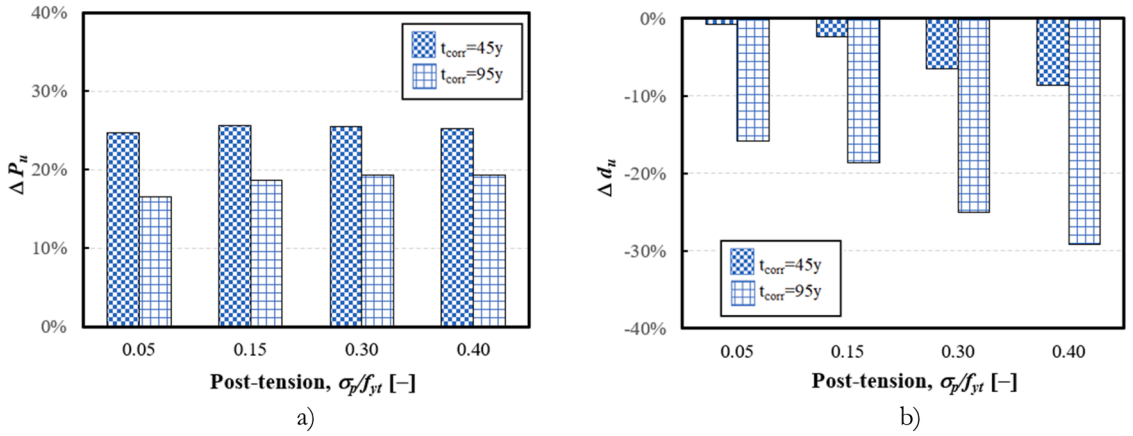

Fig. 7. Variations of ultimate load (a) and ultimate deflection (b) for retrofitted models after 45 years and 95 years of corrosion concerning the as-built corroded models (with inclined bars).

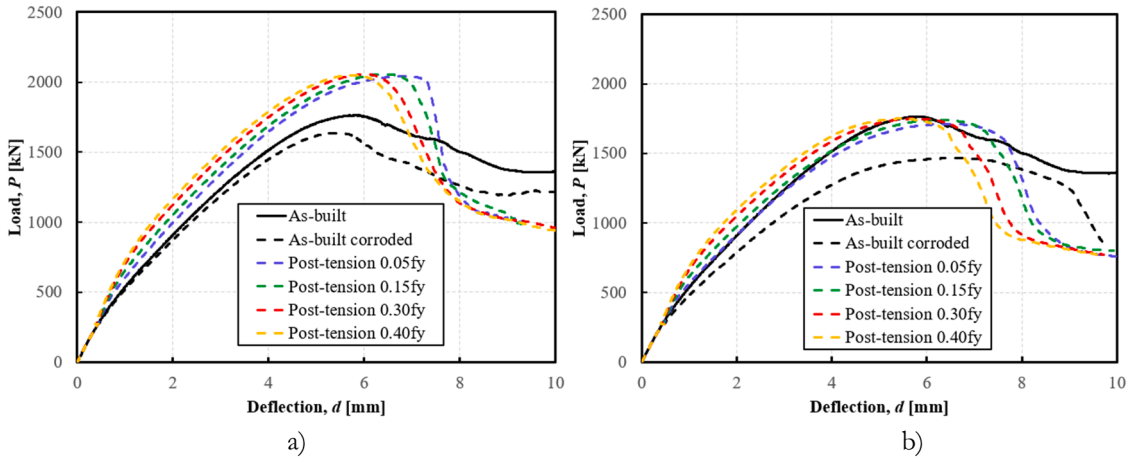

Fig. 8. Load-deflection curves of as-built and retrofitted models after 45 years (a) and 95 years (b) of corrosion (models with inclined bars).

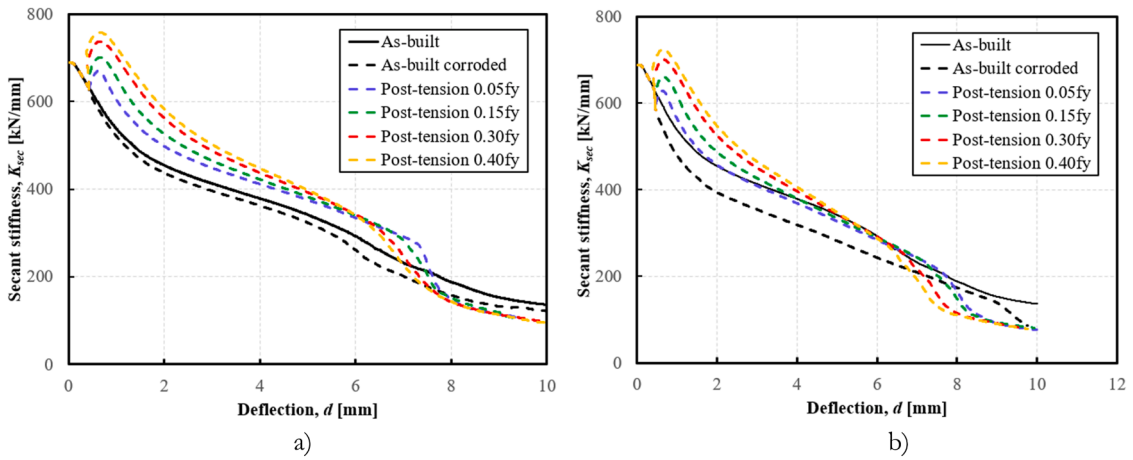

Fig. 9. Secant stiffness of as-built and retrofitted models after 45 years (a) and 95 years (b) of corrosion (models with inclined bars).

and, in case of $t_{corr} = 45$ years, to overcome by far the performance in the as-built condition. This higher strength increase could be viewed as a reserve for durability during the remaining lifespan of the structure. However, the full comparison of benefits from the application of interventions at 45 and 95 years would need a further 50 years corrosion time for the 45 years model. This analysis was not performed due to computational overhead.

Fig. 9a–b show K_{sec} of the as-built and retrofitted models. It can be noted that when post-tension becomes active, i.e. from interval 3 onward (deflection of about 0.4 mm), retrofitted models offer a significantly higher stiffness for a large part of the deflection range, i.e. until $d = 6$ mm. Once this value is overcome, due to sudden load drop, the secant stiffness of as-built models results higher.

The joint analysis of SLS and ULS behaviour leads to conclude that post-tension values σ_p/f_y should be limited in the range 0.15–0.30 to get a satisfactory performance. This result is strictly related to the half-joint at hand since it depends on the tendons' diameter and yielding stress. In order to have a more general idea of suitable post-tension values, a better choice could be made by referring to σ_c/f_{cd} ratio, which in this case should be in the range 0.14–0.27 (see Table 5).

5. Analysis of results in the absence of inclined bars

The same model analysed previously has been modified by only removing inclined rebars (see Fig. 4). Beyond the effectiveness of the post-tension intervention, this analysis case is also helpful in highlighting the contribution of inclined bars to the performance of the studied half-joint.

Table 7 shows the main results of parametric analyses similar to the previous case, as a function of the applied post-tension value σ_p/f_y for both serviceability (SLS) and ultimate limit state (ULS). First of all, the comparison of performance for $t_{corr} = 0$ reveals that the absence of inclined bars causes a loss of ultimate load of about 44 % (from 1746 to 974 kN). The cracking load P_c decreases by 49 % (from 693 to 350 kN). Moreover, the crack width observed after the application of the service load increases by about 170 %, changing from 0.0479 mm to 0.130 mm. Therefore, beyond the obvious conclusion that inclined bars significantly influence the behaviour of half-joints with respect to both serviceability and ultimate limit states, these findings confirm the similarity of results of the numerical simulation here conducted with those obtained in previous experimental tests. For example, in [9] the comparison of the test specimens with and without inclined bars showed that the latter exhibited a strength loss of about 40 %, which is very close to 44 % obtained through the present analyses.

Performance improvement at SLS when post-tension is applied (analysis from 2 to 11), is more remarkable compared to the case with inclined bars. In fact, in this case also, the cracking load is affected almost linearly by the prestress value and increments overcome 70 % with better results for $t_{corr} = 45$ y (see Fig. 10a). Moreover, the reduction of w_{max} is higher, reaching almost 50 % when post-tension stress is $0.40f_y$.

Regarding the ULS (see Fig. 11), similarly to the model with inclined bars, the ultimate load P_u shows a significant improvement even when minimum post-tension ($\sigma_p/f_y = 0.05$) is applied, remaining almost the same for higher post-tension values. This latter is between 50 % and 55 % for $t_{corr} = 45$ y and 30–35 % for $t_{corr} = 95$ y. This is in good agreement with experimental results found in the literature. In fact, specimen no. 2 tested by Atta and Taman [18] utilized a post-tension solution having the same characteristics used in this investigation that showed an ultimate load improvement, compared to the control specimen, equal to 65 % (see Section 1). In the current case, the ULS load improvement is lower (50–55 %) since corrosion degradation is considered, while Atta and Taman [18] conducted their experiments using non-corroded specimens.

Moreover, in the absence of inclined bars, interventions made after a shorter period of corrosion offer larger strength improvements.

Compared to the model with inclined bars, failure load increments are almost doubled, indicating that half-joints with this kind of steel arrangement reap the most significant benefits from post-tension interventions at ULS.

The ultimate deflection d_u increases for $t_{corr} = 45$ y, whereas it decreases for $t_{corr} = 95$ y and, in any case, it is worse for higher values of post-tension stress (Fig. 11b). The ultimate deflection of retrofitted models decreases for $t_{corr} = 95$ y due the fact that the as-built corroded model reaches the peak load for very high deflection values (caused by the larger corrosion extent) resulting in an even higher ultimate deflection value (10.61 mm). This is mainly due to the different failure modes of the as-built corroded and retrofitted

Table 7
Performance at the serviceability and ultimate limit states as a function of the applied post-tension for the model without inclined bars.

			SLS		ULS	
Analysis	t_{corr}	σ_p/f_y	P_c [kN]	w_{max} [mm]	P_u [kN]	d_u [mm]
1	0	0	350.8	0.130	974.08	8.20
2	45 years	0	312.9	0.146	880.79	6.90
3		0.05	379.5	0.137	1328.85	8.64
4		0.15	445.6	0.117	1340.58	8.51
5		0.30	515.4	0.092	1352.17	7.73
6		0.40	550.8	0.075	1354.59	7.60
7	95 years	0	282.4	0.194	751.02	10.61
8		0.05	326.6	0.183	970.96	8.40
9		0.15	365.2	0.156	1003.67	8.17
10		0.30	455.0	0.122	1029.42	7.67
11		0.40	486.1	0.100	1014.43	6.89

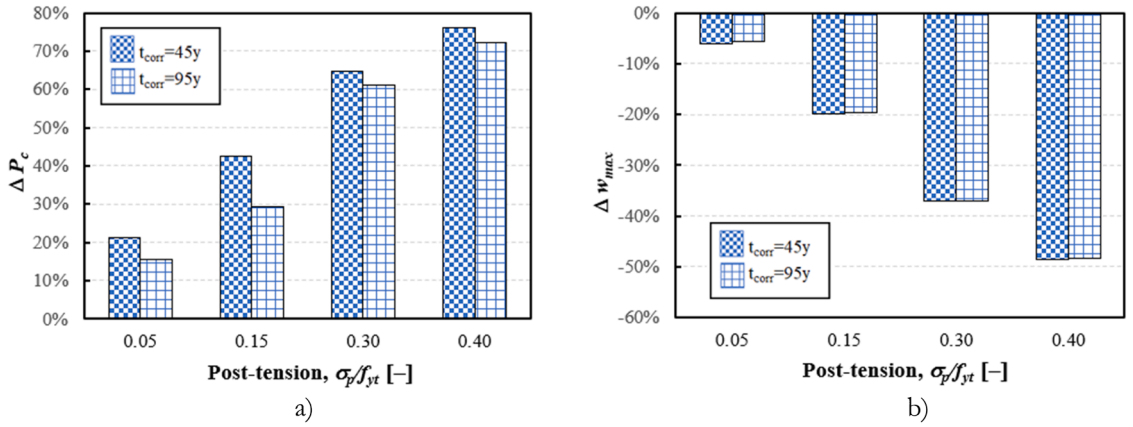

Fig. 10. Variations of cracking load (a) and maximum crack width under service loads (b) for retrofitted models after 45 years and 95 years of corrosion concerning the as-built corroded models (without inclined bars).

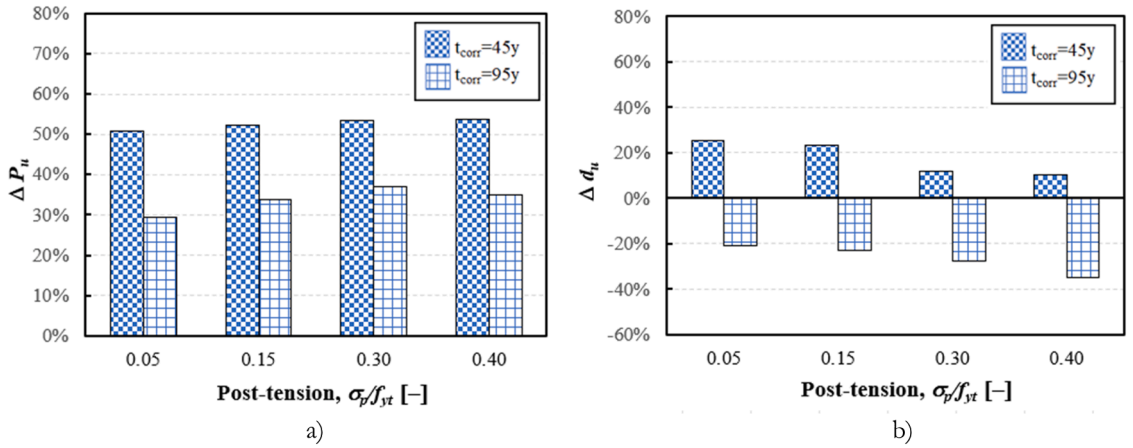

Fig. 11. Variations of ultimate load (a) and ultimate deflection (b) of retrofitted models after 45 years and 95 years of corrosion with respect to the as-built corroded models (without inclined bars).

models. As can be seen later, modes 3 and 5 (which are more ductile) occur for the as-built corroded model, while modes 2 and 4 (more brittle) occur for the retrofitted models.

Load-displacement curves depicted in Fig. 12 clearly show that interventions carried out after 45 y provide a remarkable overcome of strength with respect to the non-corroded as-built condition (Fig. 12a). Also, a remarkable increase in energy absorption is observed. In fact, the underlying area of load-deflection curves (in the retrofitted condition) is about 30 % larger than that of the as-built model. The same interventions realised after 95 y provide recovery of the original half-joint strength with negligible increments (Fig. 12b) also in terms of absorbed energy.

Fig. 13a–b show K_{sec} of the as-built and retrofitted models. In this case also, secant stiffness benefits of retrofitting interventions, especially for $t_{corr} = 45$ y since they act on a less degraded half-joint. For $t_{corr} = 95$ y a significant K_{sec} increment is observed for deflection values between 0.4 and 4 mm. However, the stiffness increase concerning the as-built corroded condition is appreciable until 8 mm deflection values.

In cases of both presence and absence of inclined rebars, after the installation of post-tension bars, the stiffness remarkably increases linearly with respect to the level of prestress. As an example, for the case of $\sigma_p/f_y = 0.40$ the stiffness increase is in the range 25–28 % for interventions made after 45 years while it is equal to 18–20 % in case the interventions are made after 95 years. In all cases, the secant stiffness starts decreasing again once the deflection reaches values of about 0.7–0.8 mm as can be seen in Fig. 13.

The results show that SLS performance is significantly sensitive to the post-tension stress values since better results in terms of cracking load improvement and crack width reduction are obtained for higher values of the tendons' initial stress. As for the model provided with inclined bars, the ultimate load improvement is not dependent on the post-tensioning amount since even for low tendons' stresses, a good performance enhancement is obtained. Generally, the model without inclined bars showed more remarkable befits from the post-tension interventions compared to the model with inclined bars. This is because vertical tendons are somehow able to overcome the lack due to the absence of inclined bars.

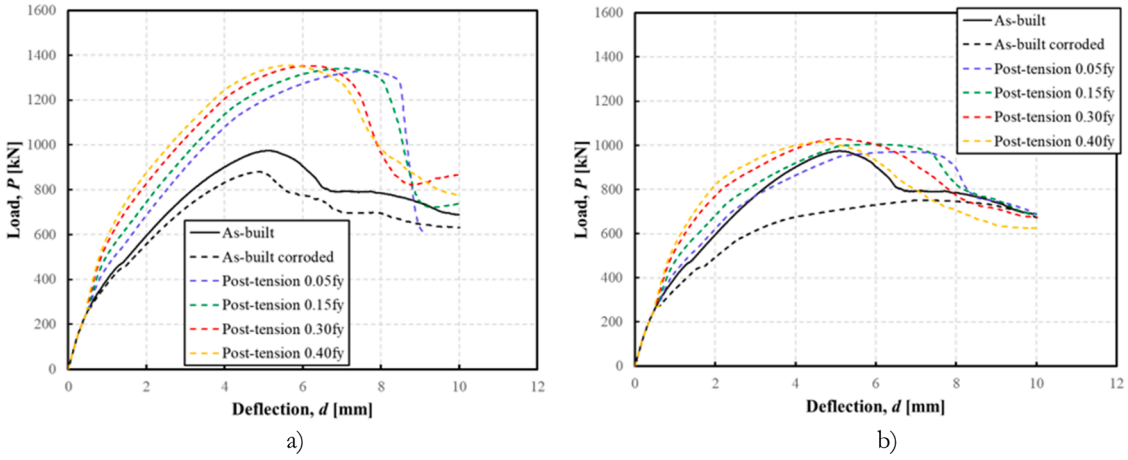

Fig. 12. Load-deflection curves of as-built and retrofitted models after 45 years (a) and 95 years (b) of corrosion (models without inclined bars).

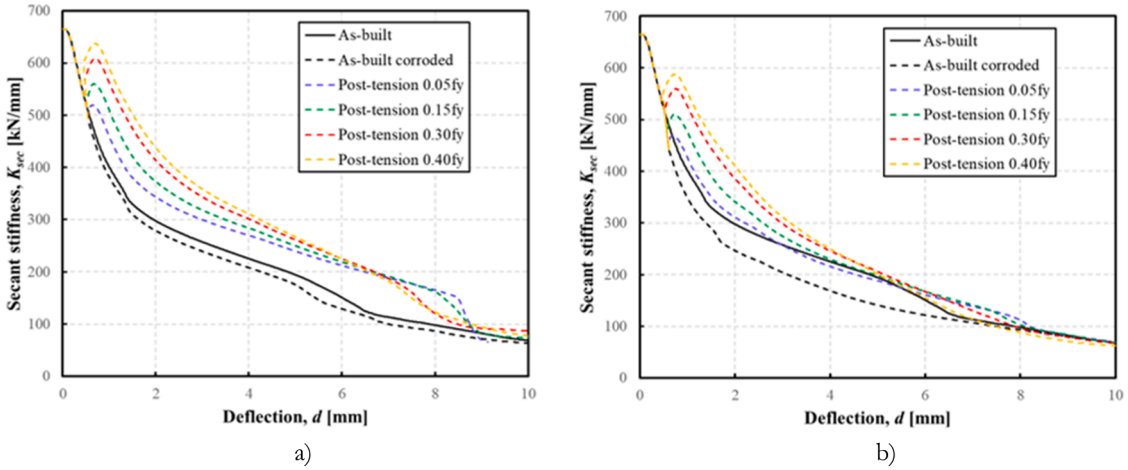

Fig. 13. Secant stiffness of as-built and retrofitted models after 45 years (a) and 95 years (b) of corrosion (without inclined bars).

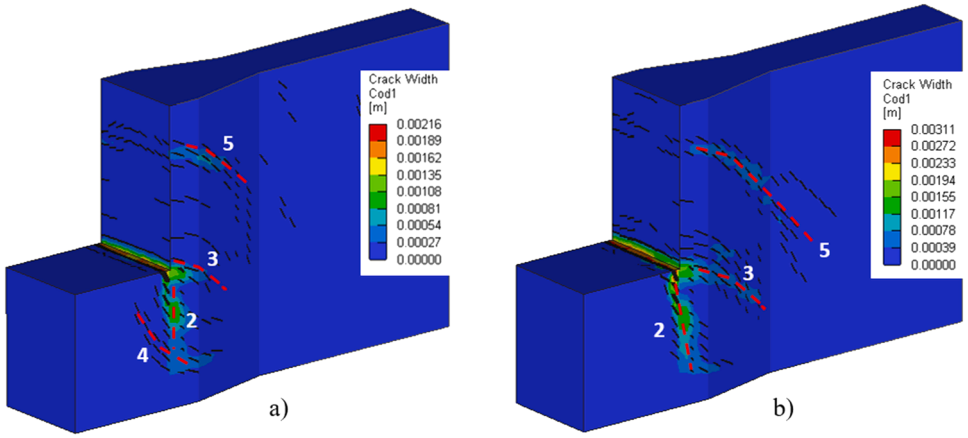

Fig. 14. Crack patterns at peak load in as-built corroded specimens with (a) and in without (b) inclined bars for t_{corr} = 95 y.

6. Analysis of failure modes

This section aims to analyse the failure modes of the studied half-joint to highlight changes caused by the post-tension intervention. For the sake of brevity, among the several cases numerically investigated, the analysis will be limited to the case of t_{corr} = 95 y, considering the higher values of post-tension (0.40f_y) in the presence and absence of inclined bars.

Fig. 14 shows the crack width colormaps at peak load for t_{corr} = 95 y in the as-built corroded condition both in the presence (Fig. 14a) and in the absence (Fig. 14b) of inclined bars. In the latter case, the predominant mechanisms (with wider cracks) are 3 (re-entrant corner crack) and 2 (direct shear) and failure mode 5 is also present (refer to Fig. 2). The maximum crack width is around 3.0 mm.

For the model with inclined bars, modes 3 and 5 occur even though they are less significant. Mode 2 is also present with some nib diagonal cracks, highlighting the concrete crushing in the dapped end according to mode 4. In this case, maximum crack width is just higher than 2.0 mm.

Now it is helpful to show the mechanisms leading to failure in the presence of post-tension interventions. For instance, Fig. 15 shows the variation of tendons' stress as a function of deflection for the minimum and maximum imposed prestress (0.05f_y and 0.40f_y), in the case of the presence and absence of inclined bars (wi = without inclined bars), considering both corrosion periods (45 y and 95 y). As can be seen, a sudden stress increase is observed at a deflection value of about 0.40 mm, corresponding to the third analysis interval start point (application of prestressing load). Then, stress grows up to the imposed values by jacking. First, it can be noted that, when lower prestress is applied, as a consequence of the external load increase, the tendons' stress undergoes a higher growth. In fact, in the cases with $\sigma_p = 0.05f_y$, which is equal to 47.5 MPa, the maximum stress reaches average values between 340 and 410 MPa (an increase of 600–700 %). On the contrary, when the applied prestress is 0.40f_y (380 MPa) the maximum stress achieves a value in the range 500–560 MPa (an increase of 30–50 %). However, the stress is always far from the yielding value of the used steel, which is equal to 950 MPa.

To carefully analyse the effect of post-tension on the mechanical behaviour and failure modes of the studied half-joint, the following colormaps show some key response indicators such as concrete principal stress, crack width and steel stress. They are shown in three specific phases: after interval 2, i.e. once the static load P_s and chloride attack have been applied; after interval 3, corresponding to the time in which the application of post-tension has been completed; at peak load during interval 4. This is done by referring to models with t_{corr} = 95 y and post-tension stress equal to 0.40f_y.

Fig. 16 shows the change in the internal stress regime just before and after the application of post-tension F_p, as well as at peak load in the presence and in absence of inclined bars. As can be seen, for both cases, post-tension can strongly reduce tensile stress values at the interface between the nib and the full-depth region of the half-joint. The presence of inclined bars (Fig. 16a–c) allows the occurrence of a wider diagonal compression strut in the nib (starting under the applied load P_s or P_u) compared to the case without them (Fig. 16d–f). At peak load, the nib compression strut is subjected to high-stress values highlighting crushing phenomena in concrete.

Fig. 17 shows the crack width in the mentioned phases. The width of cracks (according to mode 3 in Fig. 2) remarkably reduces as a consequence of post-tension. In the model with inclined bars, it passes from 0.07 mm to about 0.04 mm (Fig. 17a,b), while in the model without inclined bars it reduces from 0.19 mm to 0.10 mm (Fig. 17d,e). Therefore, the presence of inclined bars leads to a crack width about three times lower than the case without inclined bars (0.07 mm and 0.19 mm respectively).

However, the crack width is almost halved in both cases due to post-tension. At peak load, the model with inclined bars shows

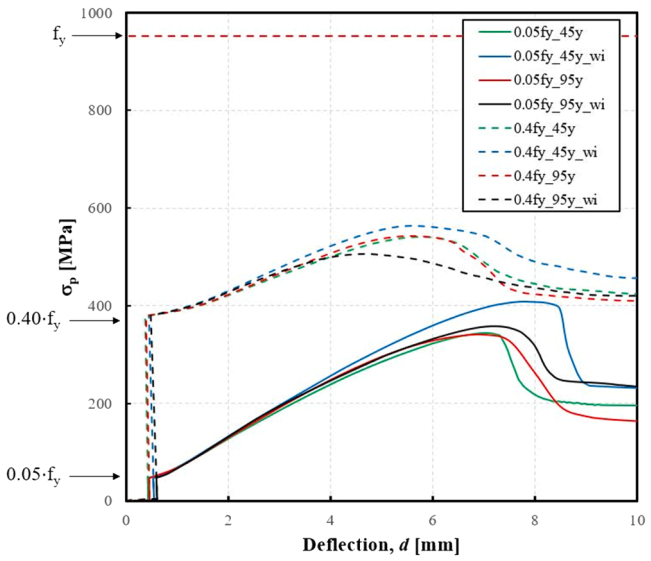

Fig. 15. Tendons' stress as a function of deflection.

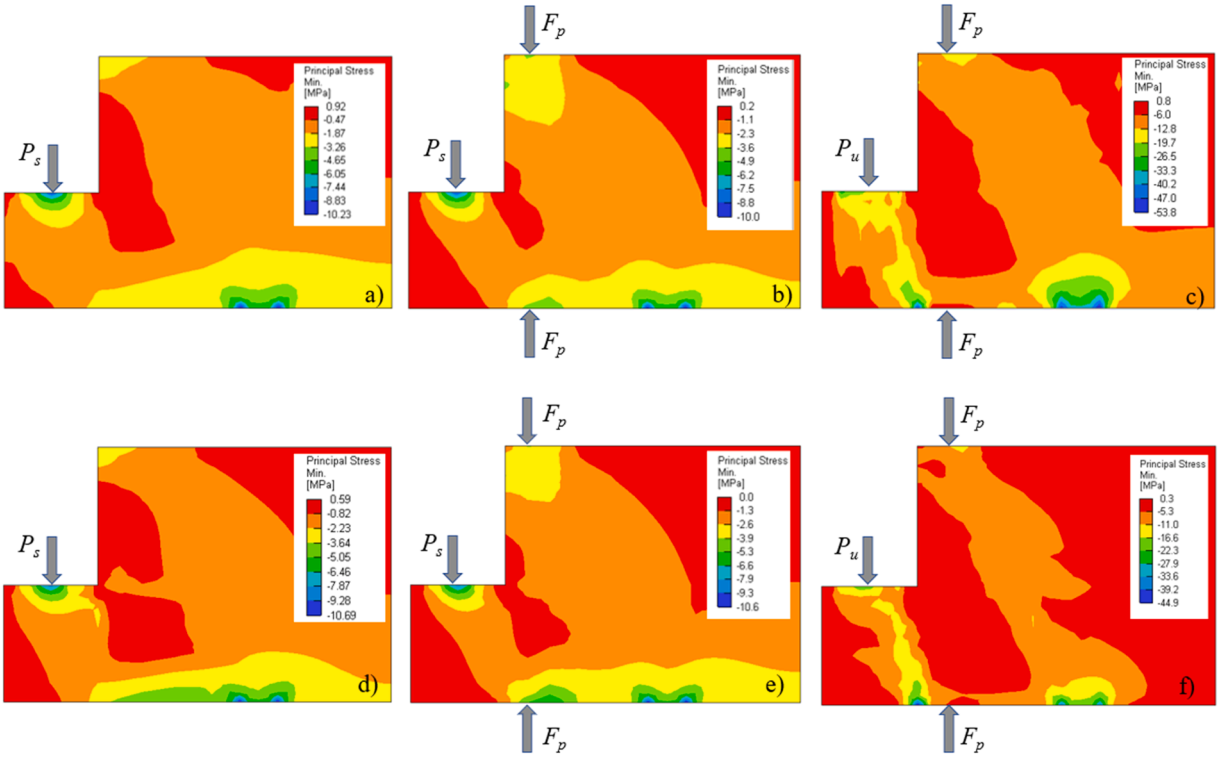

Fig. 16. Principal stress for the model with $0.40f_y$ and $t_{corr} = 95$ y in the presence (a,b,c) and in the absence of inclined bars (d,e,f): after interval 2 (a,d), after interval 3 (b,e) and in interval 4 at peak load (c,f).

negligible diagonal cracking (Fig. 17c) in the full depth region (mode 5 according to Fig. 2), inclined cracks in the nib related to concrete strut crushing (mode 4) and direct (vertical) shear cracks at the nib-full depth interface according to mode 2. Therefore, due to the inhibition of modes 3 and 5 through post-tension, the failure mode is $2 + 4$ which is mainly related to concrete crushing accompanied by lower ductility. Rather similar behaviour is shown by the model without inclined bars (Fig. 17f), even though inclined nib cracks are negligible and direct shear cracks are predominant: therefore, it is essentially a failure mode of type 2.

Fig. 18 shows the effects of post-tension in terms of steel stress reduction. It must be noted that, for the sake of simplicity, the nib confining stirrups are not shown. As can be seen, the application of post-tension can reduce steel peak stress by about 45 % for the model with inclined bars (comparing Fig. 18a and b) and by 50 % in their absence (see Fig. 18d and e). Fig. 18c shows that, at peak load in the presence of inclined reinforcement, there are yielded bars (max stress 380 MPa, just above the yielding value) while, in the absence, steel reinforcement is fully in the elastic range, as maximum stress is lower than $f_{yd} = 375$ MPa. This latter testifies that both failure mechanisms are relatively brittle and related to concrete crushing involving modes 2 and 4.

7. Conclusions

This paper numerically evaluates a post-tension rehabilitation solution for RC half-joints applied to a case study existing bridge structure accounting for corrosion deterioration. Moreover, to widen the significance of results, the half-joint at hand has also been studied with a modified reinforcement layout, i.e. removing the inclined rebars. The effectiveness of the investigated intervention is also evaluated as a function of post-tension stress applied to tendons and accounting for chloride-induced corrosion simulated through mechano-chemical analyses, considering two different periods (45 and 95 years). It is worth noting that the actual sequence of phases is considered, as each analysis considers four different intervals devoted to (i) application of the service load, (ii) chloride attack, (iii) installation and jacking of post-tension system, (iv) failure analysis under displacement control.

The main findings that can be drawn from this study are as follows:

- Performance improvement due to post-tension intervention at the serviceability limit state (e.g. increase of cracking load, P_c) is almost a linear function of the applied prestress, reaching values of 50 % and 70 % with and without inclined bars, respectively. At the same time, significant reductions in crack width under the applied load are observed after post-tension application, highlighting that this retrofitting solution can limit further deterioration due to the diffusion of corroding agents through the cracks.
- The improvement of the ultimate load-bearing capacity is almost independent of the prestress level since it was found that, even under the lower prestress value ($0.05f_y$), a significant ultimate load increase is obtained, ranging between 18–25 % in the presence of inclined bars and 30–55 % in the absence of inclined bars. The deflection capacity usually worsens as the prestress values

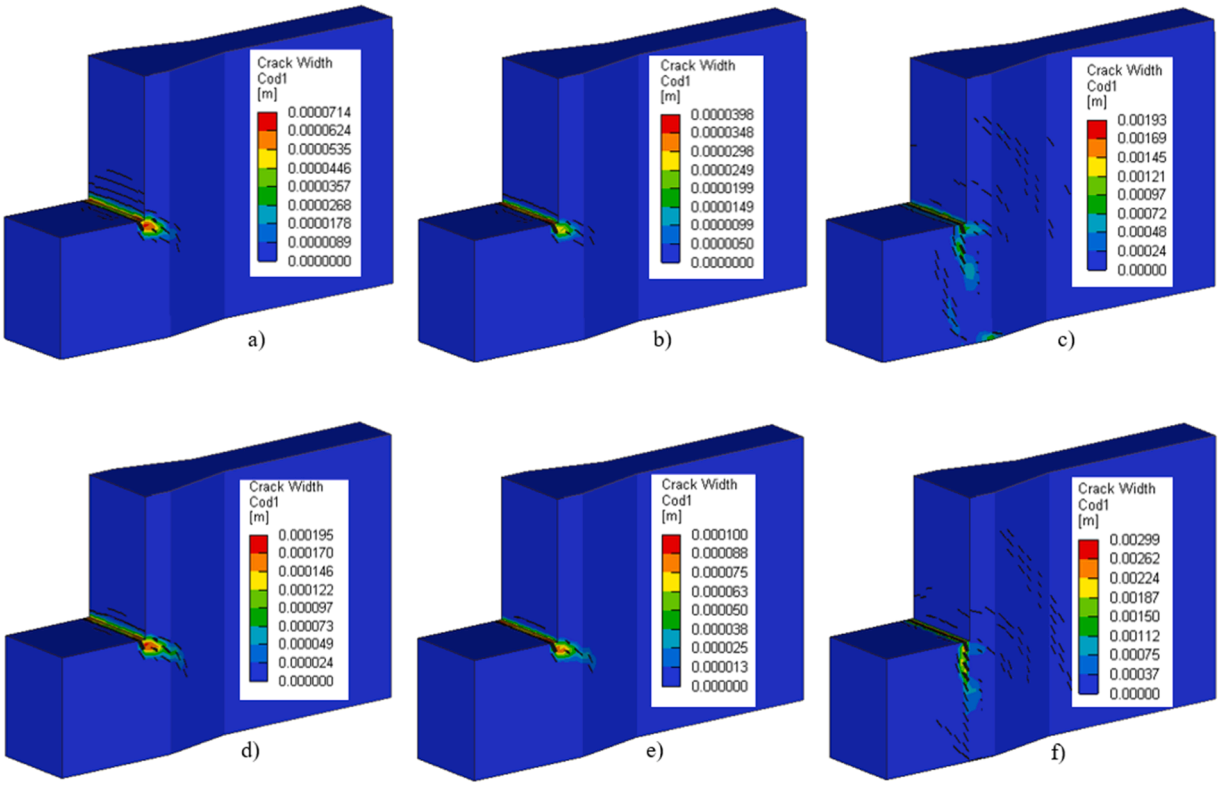

Fig. 17. Crack width for the model with $0.40f_y$ and t_{corr} = 95 y in the presence (a–c) and in the absence (d–f) of inclined bars: after interval 2 (a,d), after interval 3 (b,e) and in interval 4 at peak load (c,f).

increase since the post-tension intervention influences the failure modes. In fact, in presence of post-tension, ductile mechanisms (3 and 5) are inhibited, and failure occurs through more brittle modes (2 and 4).

- As expected, post-tension interventions made after 45 y can provide a strength recovery larger than that obtained after 95 y. However, the absolute performance obtained after 45 y and 95 y cannot be compared due to the difference in terms of corrosion time, which heavily influences the structural response.
- In all cases, the tendons' stress at peak load remains fully in the elastic range and far from the yielding value as it is desirable for an external post-tension system.
- The choice of the tendons' prestress should be made based on the main objective of the rehabilitation intervention: if the focus is on SLS, it makes sense to apply higher values (up to $0.40f_y$ for the case study at hand) which correspond to concrete compression stress values σ_c, at top and bottom half-joint surfaces, up to 36 % of concrete design strength; if the performance objective is the ULS, even small prestress values (0.05 f_y) demonstrated to be very effective in improving the half-joint response.

Even though related to a specific case study, the results of the present numerical investigation are to some extent applicable to other similar cases, given that the details here considered are rather typical concerning RC cantilever bridges. Durability is significantly improved through post-tension since, even after 95 years of corrosion, the load-bearing capacity returns to the level of the as-built condition.

Finally, it is worth remembering that corrosion simulations here presented are based on a deterministic approach requiring, as a future development, more refined analyses with stochastic assumptions related to the parameters governing the chloride ingress. This is even more important for the estimation of the chloride diffusion coefficient, which needs to be referred to the concrete of the structure at hand.

This latter can lead to carrying out reliability analyses which are the final step of probabilistic durability evaluations. Moreover, a further refinement of the study could consist in considering the moving loads in addition to the structure's self-weight as the service load acting during the corrosion analyses.

CRediT authorship contribution statement

Giuseppe Santarsiero: Conceptualization, Methodology, Investigation, Resources, Writing – original draft, Writing – review & editing, Supervision, Project administration, Funding acquisition. **Valentina Picciano:** Methodology, Software, Validation, Formal analysis, Investigation, Data curation, Writing – review & editing.

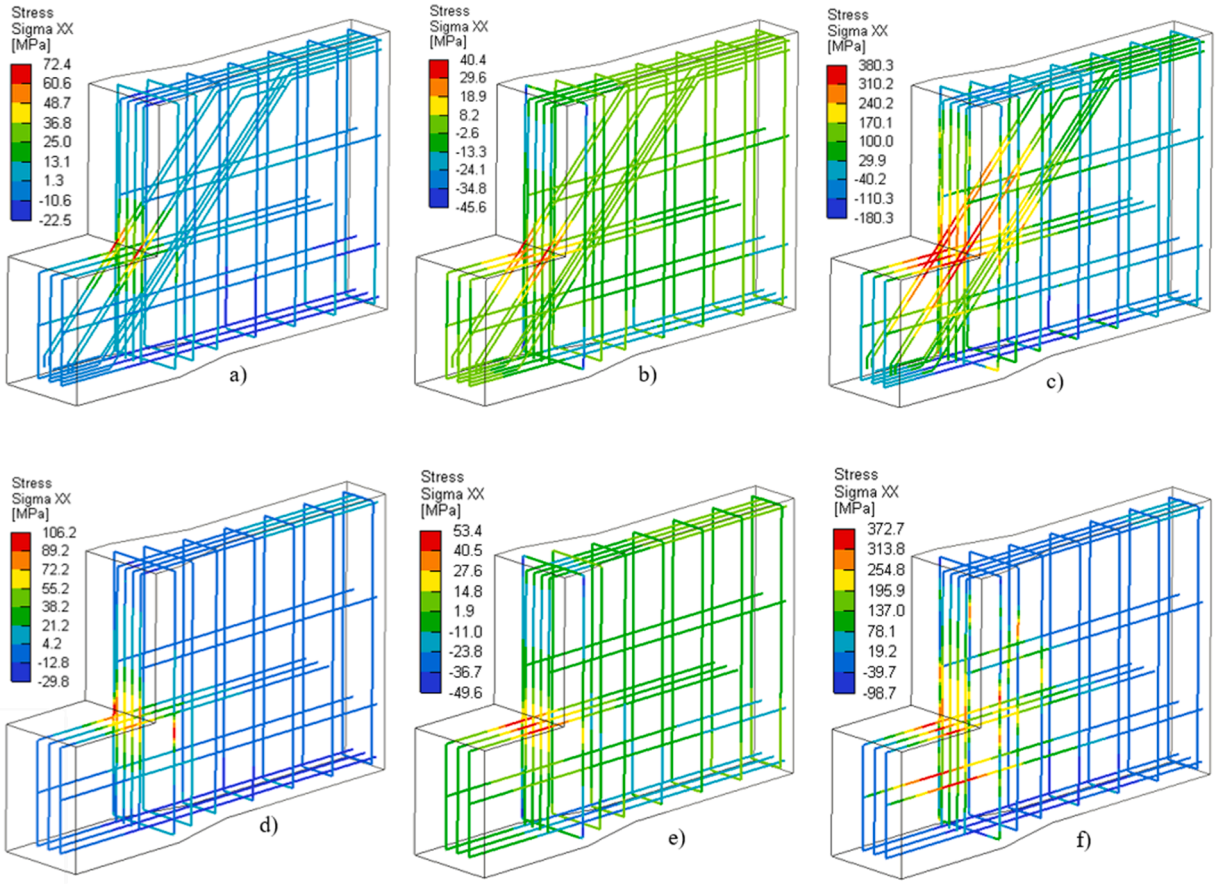

Fig. 18. Stress levels in steel reinforcement for the model with $0.40f_y$ and $t_{corr} = 95$ y in the presence (a–c) and in the absence (d–f) of inclined bars: after interval 2 (a,d), after interval 3 (b,e) and in interval 4 at peak load (c,f).

Declaration of Competing Interest

The authors declare that they have no known competing financial interests or personal relationships that could have appeared to influence the work reported in this paper.

Data Availability

No data was used for the research described in the article.

Acknowledgments

This study was partially developed under the financial support of the Italian Department of Civil Protection, within the ReLUIS-DPC 2022–2024 project (WP5, Task 5.4 “Upgrading and retrofitting interventions of existing bridges”). This support is gratefully acknowledged.

The author would like to express their gratitude to the five anonymous reviewers, which helped to improve the paper through their constructive comments.

References

[1] K. Rokneddin, J. Ghosh, L. Dueñas-Osorio, J.E. Padgett, Bridge retrofit prioritisation for ageing transportation networks subject to seismic hazards, Struct. Infrastruct. Eng. 9 (2013) 1050–1066.
[2] S. Kun, R. Vogt, O. Leuenberger, Rehabilitation of reinforced concrete Gerber bridges, in: Proceedings of the SMAR 2015 Third Conference on Smart Monitoring Assessment and Rehabilitation of Civil Structures, 2015.
[3] D.J. Lee, Bridge Bearings and Expansion Joints, Second edition, G. Maunsell & Partners, Kent, UK, 1994.
[4] J. Bernal, M. Fenaux, A. Moragues, E. Reyes, J.C. Gálvez, Study of chloride penetration in concretes nexposed to high-mountain weather conditions with presence of de-icing salts, Constr. Build. Mater. 127 (2016) 971–983.
[5] O.E. Gjørv, Durability Design of Concrete Structures in Severe Environments, Taylor & Francis, London, UK; New York, NY, USA, 2009.

[6] D. Mitchell, J. Marchand, P. Croteau, W. Cook, Concorde overpass collapse: structural aspects, J. Perform. Constr. Facil. 25 (2011) 545–553.
[7] G. Santarsiero, A. Masi, V. Picciano, Durability of Gerber saddles in RC bridges: analyses and applications (Musmeci Bridge, Italy), Infrastructures 6 (2021) 25, https://doi.org/10.3390/infrastructures6020025.
[8] P. Desnerck, J.M. Lees, C.T. Morley, Strut-and-tie models for deteriorated reinforced concrete half-joints, Eng. Struct. 161 (2018) 41–54, https://doi.org/10.1016/j.engstruct.2018.01.013.
[9] Desnerck Pieter, J.M. Lees, C.T. Morley, Impact of the reinforcement layout on the load capacity of reinforced concrete half-joints, Eng. Struct. 127 (2016) 227–239, https://doi.org/10.1016/j.engstruct.2016.08.061.
[10] P. Lehner, M. Horňáková, K. Hrabová, Sensitivity analysis of stochastic calculation of SCC regarding aggressive environment, Materials 14 (2021) 6838, https://doi.org/10.3390/ma14226838.
[11] Q.C. Truong, C. El Soueidy, Y. Li, E. Bastidas-Arteaga, Probability-based maintenance modeling and planning for reinforced concrete assets subjected to chloride ingress, J. Build. Eng. 54 (2022), 104675, https://doi.org/10.1016/j.jobe.2022.104675.
[12] R.Z. Al-Rousan, M.A. Alhassan, E.A. AlShuqari, Behavior of plain concrete beams with DSSF strengthened in flexure with anchored CFRP sheets—effects of DSSF content on the bonding length of CFRP sheets, Case Stud. Constr. Mater. 9 (2018), e00195, https://doi.org/10.1016/j.cscm.2018.e00195.
[13] R.Z. Al-Rousan, Behavior of macro synthetic fiber concrete beams strengthened with different CFRP composite configurations, J. Build. Eng. 20 (2018) 595–608, https://doi.org/10.1016/j.jobe.2018.09.009.
[14] P.C. Huang, A. Nanni, Dapped-end strengthening of full-scale prestressed double tee beams with FRP composites, Adv. Struct. Eng. 9 (2) (2006) 2006.
[15] S.E.-D.F. Taher, Strengthening of critically designed girders with dapped ends January 2005ICE Proceedings Structures and Buildings, vol. 158(no. 2), 2005, pp. 141–52. ⟨https://doi.org/10.1680/stbu.2005.158.2.141⟩.
[16] T. Nagy-Gyorgy, G. Sas, A.C. Daescu, J.A.O. Barros, V. Stoian, Experimental and numerical assessment of the effectiveness of FRP-based strengthening configurations for dapped-end RC beams, Eng. Struct. 44 (2012) 291–303.
[17] PCI Design Handbook: Precast and Prestressed Concrete, Sixth Edition, 2010.
[18] A. Atta, M. Taman, Innovative method for strengthening dapped-end beams using an external prestressing technique, Mater. Struct. 49 (2016) 3005–3019, https://doi.org/10.1617/s11527-015-0701-8.
[19] L. Lafranconi, G. Massone, G. Pasqualato, Analysis and rehabilitation of the Generale Franco Romano viaduct, in: Proceedings of the Italian Concrete Days 2018, CTE Conference Milano/Lecco 13–16 Giugno 2018, 2018.
[20] M. Di Prisco, Critical infrastructures in Italy: state of the art, case studies, rational approaches to select the intervention priorities, in: Proceedings of the Fib Symposium 2019: Concrete – Innovations in Materials, Design and Structures.
[21] F. Marmo, C. Demartino, G. Candela, C. Sulpizio, B. Briseghella, R. Spagnuolo, Y. Xiao, I. Vanzi, L. Rosati, On the form of the Musmeci's bridge over the Basento river, Eng. Struct. 191 (2019) 658–673.
[22] F.C. Ponzo, A. Di Cesare, M. Dolce, C. Moroni, D. Nigro, G. Auletta, R. Ditommaso, Vulnerabilità Sismica del ponte "Musmeci" a Potenza, Progett. Sismica 4 (2013) 3.
[23] F. Alessandrini, P. Burba, Il degrado strutturale degli appoggi. Rassegna tecnica del Friuli-Venezia-Giulia, N.4/1994, Anno XLIV, 1994. (in Italian).
[24] B.S. Mohammed, M. Aswin, M.S. Liew, Prediction of failure load of RC and R-ECC dapped-end beams, Case Stud. Constr. Mater. 13 (2020), e00433.
[25] J. Mata-Falcón, L. Pallarés, P.F. Miguel, Proposal and experimental validation of simplified strut-and-tie models on dapped-end beams, Eng. Struct. 183 (2019) 594–609.
[26] A.H. Mattock, T.C. Chan, Design and behavior of dapped-end beams, PCI J. 24 (6) (1979) 28–45.
[27] W.Y. Lu, I.J. Lin, H.W. Yu, Behaviour of reinforced concrete dapped-end beams, Mag. Concr. Res. 64 (9) (2012) 793–805.
[28] W.Y. Lu, I.J. Lin, S.J. Hwang, Y.H. Lin, Shear strength of high-strength concrete dapped-end beams, J. Chin. Inst. Eng. 26 (5) (2003) 671–680.
[29] S. Ahmad, A. Elahi, J. Hafeez, M. Fawad, Z. Ahsan, Evaluation of the shear strength of dapped ended beam, Life Sci. J. 10 (3) (2013) 1038–1044.
[30] M. Aswin, B.S. Mohammed, M.S. Liew, Z.I. Syed, Shear failure of RC dapped-end beams, Adv. Mater. Sci. Eng. (2015) 2015.
[31] W.Y. Lu, T.C. Chen, I.J. Lin, Shear strength of reinforced concrete dapped-end beams with shear span-to-depth ratios larger than unity, J. Mar. Sci. Technol. 23 (4) (2015) 431–442 (5).
[32] H.N. Hussain, Q.M. Shakir, Experimental study of the behavior of reinforced concrete beams with composite dapped end under effect of static and repeated loads, Int. J. Appl. Sci. 2 (2019) 1.
[33] Q. Wang, Z. Guo, P.C. Hoogenboom, Experimental investigation on the shear capacity of RC dapped end beams and design recommendations, Struct. Eng. Mech. 21 (2) (2005) 221–235.
[34] J.Y. Moreno-Martínez, R. Meli, Experimental study on the structural behavior of concrete dapped-end beams, Eng. Struct. 75 (2014) 152–163.
[35] G. Santarsiero, V. Picciano, A. Masi, Structural rehabilitation of half-joints in RC bridges: a state-of-the-art review, Submitt. Struct. Infrastruct. Eng. (2022).
[36] Circolare n. 384 del 1962 del Ministero LL.PP, "Norme relative ai carichi per il calcolo dei ponti stradali" (Ministero dei Lavori Pubblici).
[37] Antonio Bossio, Gian Piero Lignola, Andrea Prota, An overview of assessment and retrofit of corroded reinforced concrete structures, Procedia Struct. Integr. 11 (2018) 394–401, https://doi.org/10.1016/j.prostr.2018.11.051 (ISSN 2452-3216).
[38] U.M. Angst, Predicting the time to corrosion initiation in reinforced concrete structures exposed to chlorides, Cem. Concr. Res. 115 (2019) 559–567.
[39] Ministry of Infrastructure, CSLP, Guidelines on Risk Classification and Management, Safety Assessment and Monitoring of Existing Bridges, Ministry of Infrastructure, Rome, Italy, 2020. (in Italian).
[40] J. Cervenka, K. Hajkova, L. Jendele, T. Sajdlova, V. Smilauer, Durability assessment of reinforced concrete structures assisted by numerical simulation, in: Proceedings of the 71st RILEM Annual Week & ICACMS 2017, Chennai, India, 2017.
[41] J. Zhang, J. Wang, D. Kong, Chloride diffusivity analysis of existing concrete based on Fick's second law, J. Wuhan Univ. Technol. 25 (2010) 142–146.
[42] L. Bertolini, B. Elsener, P. Pedeferri, R. Polder, Corrosion of Steel in Concrete, Prevention, Diagnosis, Repair, WILEY-VCH Verlag GmbH & Co. KGaA, Weinheim, Germany, 2004.
[43] K. Hájková, V. Šmilauer, L. Jendele, J. Červenka, Prediction of reinforcement corrosion due to chloride ingress and its effects on serviceability, Eng. Struct. 174 (2018) 768–777.
[44] G. Van derWegen, R.B. Polder, K. Van Breugel, Guideline for service life design of structural concrete—a performance based approach with regard to chloride induced corrosion, Heron 57 (2012) 153–168.
[45] G. Santarsiero, A. Masi, Analysis of slab action on the seismic behavior of external RC beam-column joints, J. Build. Eng. 32 (November 2020) (2020), 101608.
[46] Cervenka Consulting, ATENA Program Documentation, Part 1, ATENA Theory Manual, 2000–2014.
[47] Z.P. Bazant, B.H. Oh, Crack band theory for fracture of concrete, Mater. Struct. 16 (1983) 155–177.
[48] Fib, Fédération Internationale du Béton, Model Code 2010 First Complete Draft, Fib Bulletin n. 55, vol. 1, Lausanne, Switzerland, 2010;.
[49] EN 1993-1-1 (2005) (English): Eurocode 3: Design of Steel Structures – Part 1-1: General Rules and Rules for Buildings [Authority: The European Union Per Regulation 305/2011, Directive 98/34/EC, Directive 2004/18/EC].
[50] NTC2018 – Ministry of Infrastructure, DM 17 gennaio 2018: Aggiornamento delle Norme tecniche per le costruzioni, Suppl. or. n.30 alla G.U. n.29 del 4/2/2008 (in Italian), 2018. (in Italian).
[51] EN 1992-1-1 (2004) (English): Eurocode 2: Design of Concrete Structures – Part 1-1: General Rules and Rules for Buildings, Authority: The European Union Per Regulation 305/2011, Directive 98/34/EC, Directive 2004/18/EC].
[52] T.B. Panagiotakos, M.N. Fardis, Deformation of reinforced concrete members at yielding and ultimate, ACI Struct. J. 98 (2) (2001) 135–148.